Applied Physics, Material Sciences, and Engineering Journal
ISSN 3065-1425
Volume 13 Issue 2
April-June 2025
Impact Factor: 8.13
Enquiry: contact@continentalpub.online
Published by Continental Publication | https://cspjournals.org/index.php/apmsej

MODELING MAGNETIC DIPOLES IN DIELECTRIC RINGS WITH THE BIOT–SAVART–LAPLACE FRAMEWORK

Alexei Mikhail Sergeyev
Theoretical Physics and Quantum Technologies Department, National University of Science and Technology MISIS, 119049 Moscow, Russia

Abstract: *We investigate the electromagnetic response of a high-permittivity dielectric plane ring under GHz-frequency plane wave excitation. Our results demonstrate that the ring behaves as an almost ideal magnetic dipole at its fundamental resonance, with negligible contributions from higher-order multipoles—less than 0.2% of the primary magnetic dipole component. Experimental measurements of the magnetic field distribution around the ring align closely with both numerical simulations and predictions based on the Biot–Savart–Laplace law. This confirms that the Biot–Savart–Laplace framework, traditionally applied to conductive metal rings, is also valid for accurately modeling non-conductive, low-loss dielectric structures at microwave frequencies. These findings offer a new route for engineering low-loss, magnetically resonant dielectric elements for use in advanced electromagnetic and metamaterial systems.*

Keywords: *Dielectric ring, Magnetic dipole resonance, GHz scattering*

I. INTRODUCTION

Recently, the resonant excitation of magnetic modes as well as demonstration of negative magnetic inductance in subwavelength plasmonic and all-dielectric structures gained a lot of interest from microwave to optics. Importantly, for plasmonic systems, the main resonance and higher order resonances are limited by metal associated large dissipation losses[1] that is more significant in the visible range. Substitution metals by all-dielectric structures allows avoiding large dissipative losses which has been theoretically shown[2,3] and experimentally demonstrated.[4,5] High-index all-dielectric structures of subwavelength scale provide strong magnetic response by impinging electromagnetic waves. Nowadays, the study of possibility of light manipulation in subwavelength all-dielectric structures, namely, amplitude and phase controlling is promising scientific field. Besides, all-dielectric nanophotonics as well as THz and microwave ranges related research areas are established and mainly focused on controlling electromagnetic resonances of high-index all-dielectric particles. The presence of series of electric and magnetic resonances with an opportunity to control their amplitudes and phases opens the way to majority of unique electromagnetic properties such as strong field localization in near zone,[3,6–11] enhanced radiation directivity,[12–14] nonradiating anapole modes[15–22] as well as creation of low-loss transmission lines.[23,24] Consequently, alldielectric resonant structures are being a promising platform for a number of

Vol. 13 No. 2 | Imp. Factor: 8.13
DOI: https://doi.org/10.5281/zenodo.15845927
applications of nanophotonics,[25,26] highly sensitive and highly directional antennas,[27–30] magnetic mirrors,[31–34] resonators,[30,35] polarization-dependent passive switches,[36] metasurfaces,[37,38] and meta-elements of various geometries enabling verification of theoretical calculations with the help of experimental results in a wide frequency range.[39–41] Application of all-dielectric particles as a source of magnetic dipole moment is feasible due to possibility of strong magnetic fields concentrating in their origin, as it shown in silicon nano-spheres (magnetic light), which is important for magnetic hot-spots such as nano-optomechanics, controlling of magnetic fields and enhancement of magnetic Purcell effect.[4,26] First of all, metal coils (SRR, split ring resonator) have been used for the design of metamaterials.[42,43] SRR resonant frequency can be calculated from capacitance and self-inductance, while magnetic field can be found from the Biot–Savart–Laplace law. SRR paved the way for a plenty of microwave design. It is naturally assumed that dielectric ring possesses can be assumed as the same magnetic dipole instead of. This kind element could be readily applied in structures based on metallic SRR. However, dielectric rings allow concentrating magnetic fields in the accessible free-space region.[44] Moreover, the all-dielectric rings are the platform for giant magnetoelectric field separation and anapole state excitation.[45] Due to magnetic response of dielectric rings, its response can be advantageously used in the design of negative effective permeability. Combined with dielectric rods, dielectric rings provide 3D isotropic left-handed metamaterials.[46]

The concept of dielectric magnetic dipole is widely used by analogy with a magnetic dipole created by conductive currents flowing in loops. This geometry conditioned by displacement currents flowing through thin dielectric rings. Accordingly, magnetic field distribution in the dielectric magnetic dipole is represented by analogy with the magnetic field of a conducting ring with a uniform current distribution over the cross section. However, the applicability of concepts of self-inductance for dielectric annular contour as well as the Biot–Savart–Laplace law is still questioned.

Vector of magnetic induction can be calculated from the Biot–Savart–Laplace law based on the distribution of magnetic field induction that empirically measured by Biot and Savart in 1820,[47,48] and fundamental law of electrodynamics that determines magnetic field induction created by a linear current element.[49] In vector notation, the Bio–Savart–Laplace law[50] (in SI units) is

H(r) ¼ ððð JdV r/4πr³, (1)

where is the volume element, r is the vector from dV to the observation point, the length of vector r, and J is the current density vector in that volume (in SI in units of A/m²). However, the absence of experimental verification for displacement currents led to fact that the Biot–Savart–Laplace law was formulated only for conductivity currents. The magnetic flux through the circuit is determined by current and self-inductance depending on circuit geometry. There is no clear concept of self-inductance for dielectric circuits. Therefore, its applicability for displacement currents for alternating fields is still questioned. Consequently, applicability of all-dielectric rings with displacement currents for an ideal magnetic dipole is also relevant.

In this paper, we experimentally and computer simulation study the electromagnetic response of the dielectric ring with high permittivity excited by an incident plane electromagnetic wave of the GHz range in order to show the applicability of the law of selfinduction not only for magnetic dipoles with electric conduction currents, but also for dielectric magnetic dipoles with displacement currents.

Applied Physics, Material Sciences, and Engineering Journal
Vol. 13 No. 2 | Imp. Factor: 8.13
DOI: https://doi.org/10.5281/zenodo.15845927

II. METHODS

A. Experiment

To verify the results of computer modeling, we used a flat dielectric ring with internal and external diameters of 28 and 38 mm, respectively, and a square cross section of 5 × 5 mm. This ring was fabricated from ceramics based on titanate (TiO_2, $BaTiO_3$, $SrTiO_3$). Such ceramics are usually used to manufacture high-voltage K15U-2 capacitors with a permittivities varying in the range $\varepsilon = 130–180$ and with a small loss tangent in the range $\tan\delta = 10^{-4}–10^{-3}$. The results of measuring our ceramics at a frequency of 1 kHz showed that the permittivity $\varepsilon = 150 \pm 3$ and the loss tangent $\tan\delta = 3 \times 10^{-4} \pm 3 \times 10^{-6}$. This loss tangent practically does not change up to a frequency of 1 GHz and increases significantly only at the frequencies of more 10 GHz. [51] The dielectric ring was excited by a pseudo-plane electromagnetic wave. The scheme of the experimental setup is shown in Fig. 1. The Agilent E5071C ENA network analyzer (1) was used to generate and register radiation spectra in the GHz band. The output power of the transmitter was 10 mW. To improve the signal-to-noise ratio, we used a broadband amplifier (2) with a gain coefficient of 20 dB. The twosided waveguide horn antenna ETS-Lindgren model 3115 (3) was used as the emitter. We measure the magnetic field using a magnetic field probe Beehive Electronics 100B EMC Probe (4) with a ring diameter of 0.37 cm (4), which made it possible to measure not only the scattering spectrum of the ring, but also the spatial distribution of this spectrum with a positioning accuracy of at least 0.2 cm. The distance between the antenna and the ring was 40 cm.

To eliminate radio frequency environmental noise, the radiating antenna, the test ring, and the probe were placed in an anechoic chamber equipped with ECCOSORB absorbers. To obtain a spatial distribution pattern of scattered radiation, we moved the probe (4) in space using a three-coordinate

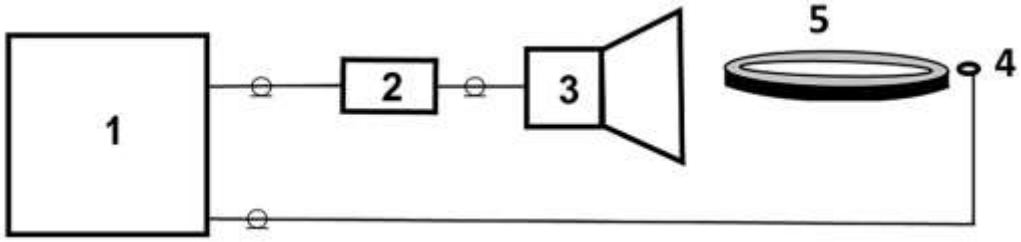

FIG. 1. Experimental setup scheme. 1—network analyzer; 2—RF broadband amplifier; 3—double ridged waveguide horn antenna; 4—circular magnetic probe; 5—planar dielectric ring.

linear positioning system. Before making the measurements, the plane of the ring and the plane of the probe were adjusted perpendicular to the vector of the magnetic field of the radiation incident from the antenna. In this case, the probe registers the magnitude of the magnetic flux passing through its ring. In our case, these are the magnetic field fluxes (H_0) of the incident radiation and the magnetic field (H) scattered by the ring. The magnetic field vector H_0 is always perpendicular to the probe plane, and the angle of the magnetic field vector H changes as the probe moves in space. In our experiments, the spectrum analyzer measures the power attenuation coefficient in decibels (dB). Therefore, in our case, we register a decrease in the power of the magnetic component of the detected radiation. At each measurement point, we measure the signal power with and without the test ring. To extract the power scattered by the ring (α), an algebraic addition of two quantities is performed.

B. Simulation

Vol. 13 No. 2 | Imp. Factor: 8.13
DOI: https://doi.org/10.5281/zenodo.15845927

Calculations for studying the scattering pattern of an incident plane electromagnetic wave by a dielectric ring were performed using the CST Microwave Studio program by solving partial differential equations. The finite-difference time-domain method was used to perform numerous calculations over a large frequency range. In simulations, we use open boundary conditions. A mesh is 10 cells per wavelength in the material. We use a frequency domain solver.

The simulation duration is 100 pulses. Convergence check means checking the amount of energy in the system—the simulation runs until the energy remaining in the system is −60 dB from the initial amount.

III. RESULTS AND DISCUSSION

Experimental and simulation dependencies of radar cross sections (RCSs) in the frequency range from 1 to 4 GHz are shown in Fig. 2. The spectra were measured at 1 mm distance from the ring to probe which plane is perpendicular to magnetic component H_0 of the incident wave. The first resonant peak corresponds to a magnetic dipole. This peak is observed at f = 1.32 GHz that wellcoincided with simulated resonance at 1.31 GHz (Fig. 2). This difference is justified by measurement error of dielectric permittivity of ring at a frequency of 1 GHz and decrease of this value with the increase of frequency. Resonant frequency is calculated by the Thompson formula for resonant contour with capacity and selfinductance providing uniform distribution of current density in lateral cross section of the ring and relative error 1%. The resonances of the magnetic quadrupole, electric dipole, and electric quadrupole are located in the frequency range of 3.2–3.5 GHz. In a wider frequency range up to 6 GHz, new resonances are observed in which high-order multipoles up to and including the magnetic octopole will be excited.

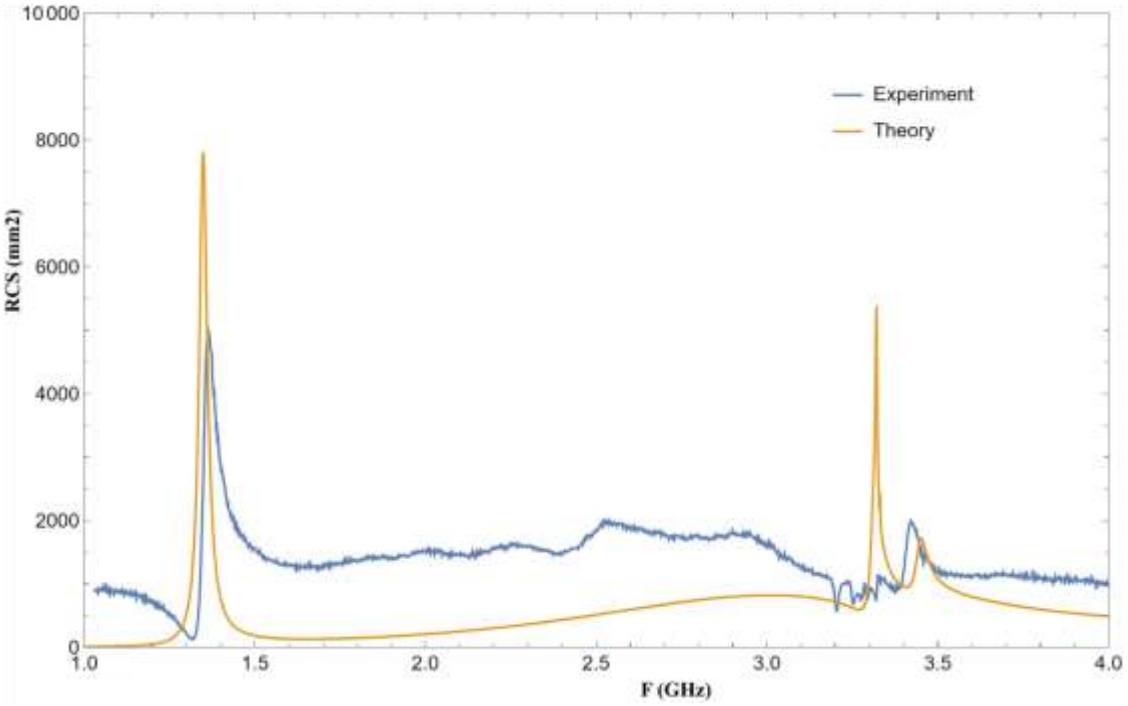

Vol. 13 No. 2 | Imp. Factor: 8.13
DOI: https://doi.org/10.5281/zenodo.15845927

FIG. 2. Experimental and simulation dependencies of radar cross sections (RCSs). Simulated—brown; experimental—blue.

Actually, the magnetic and electric fields of a plane wave can initiate in the ring not only the basic magnetic dipole resonance, but also other resonances such as electric dipole, magnetic, and electric quadrupoles, these resonances occur at higher frequencies. The magnetic and electric fields from these resonances will add up, so the resulting magnetic field of the ring scattering will differ from the distribution for an ideal magnetic dipole.

Figure 3 shows calculated magnetic field distributions in the central plane of the ring section and the radiation pattern for resonances of the magnetic dipole [Fig. 3(a)], magnetic quadrupole and electric dipole [Fig. 3(b)], electric quadrupole [Fig. 3(c)].

We calculated multipoles moments and RCS in long-wavelength approximation.

Applied Physics, Material Sciences, and Engineering Journal
Vol. 13 No. 2 | Imp. Factor: 8.13
DOI: https://doi.org/10.5281/zenodo.15845927

The system is illuminated by a plane wave, then Radar cross section (RCSs) can be approximated as

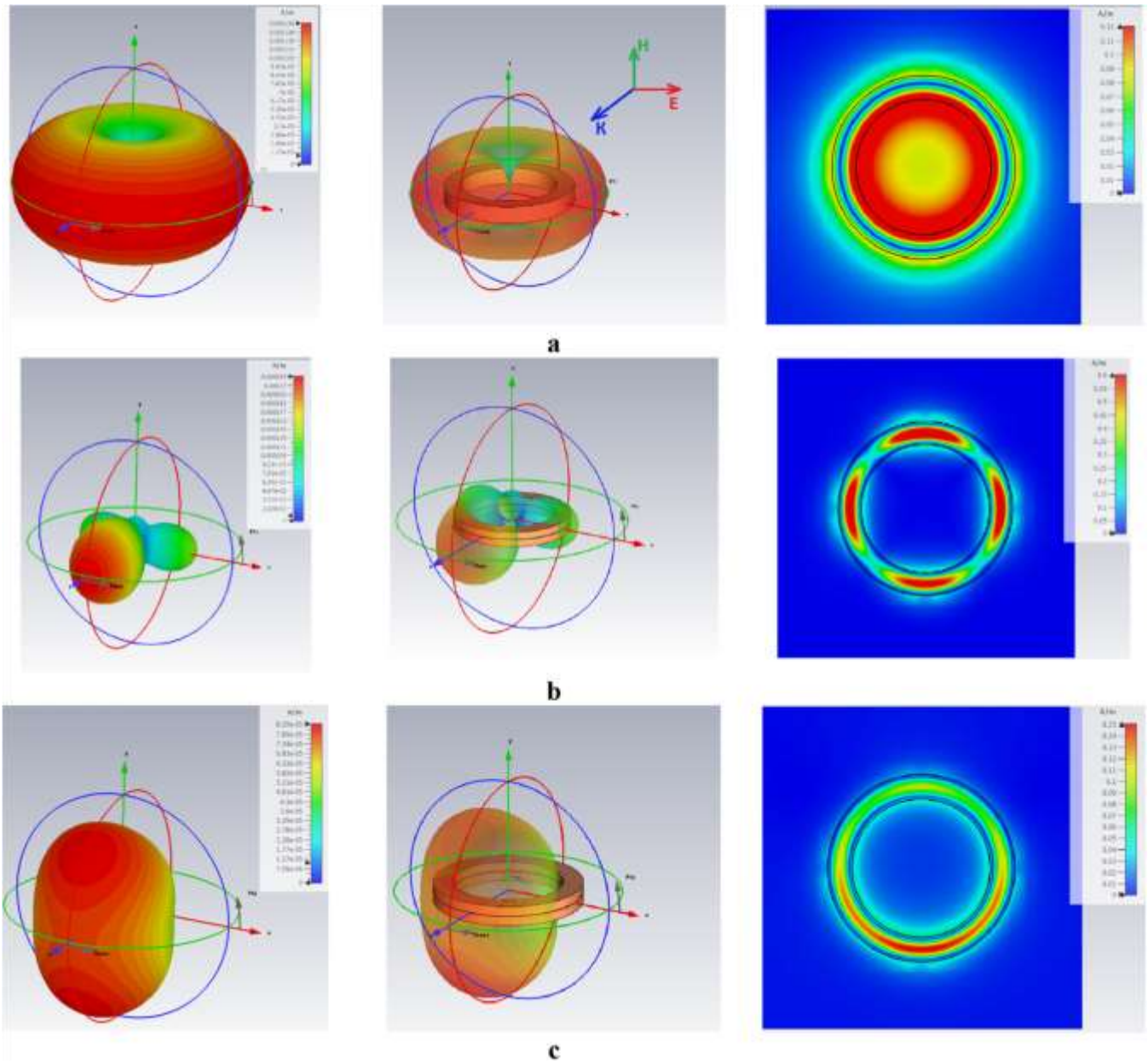

FIG. 3. Vector form distribution of the magnetic field in the plane of the longitudinal section at h = 0 of the ring and patterns of radiated magnetic field at the different frequencies. (a) Magnetic dipole 1.32 GHz, (b)magnetic quadrupole and electrical dipole, (c) electrical quadrupole.

Vol. 13 No. 2 | Imp. Factor: 8.13
DOI: https://doi.org/10.5281/zenodo.15845927

$$RCS \simeq \frac{k_0^4}{6\pi\varepsilon_0^2 |E|^2} |p|^2 + \frac{k_0^4 \varepsilon_s \mu_0}{6\pi\varepsilon_0 |E|^2} |m|^2 + \frac{k_0^6 \varepsilon_s}{720\pi\varepsilon_0^2 |E|^2} \sum_{\alpha\beta} |Q_{\alpha\beta}|^2$$
$$+ \frac{k_0^6 \varepsilon_s}{720\pi\varepsilon_0^2 |E|^2} \sum_{\alpha\beta} |Q_{\alpha\beta}|^2 + \frac{k_0^6 \varepsilon_s^2 \mu_0}{80\pi\varepsilon_0 |E|^2} \sum_{\alpha\beta} |M_{\alpha\beta}|^2, \quad (2)$$

where the multipole moments can be calculated as

$$P = -i\omega \int_V j dr,$$

$$m = \frac{1}{2} \int_V [r \times j] dr,$$

$$Q_e = \frac{3}{2i\omega} \int_V [r(r \cdot j) + (r \cdot j)r - 2r^2 j] dr,$$

$$Q_m = \frac{1}{3} \int_V ([r \times j] \otimes r + r \otimes [r \times j]) dr,$$

where c is the speed of light in vacuum, P, m, Q_e, Q_m are the electric dipole (ED), magnetic dipole (MD), electric quadrupole (EQ), and magnetic quadrupole (MQ) moments, respectively. Using Eq. (2), one can analyze the individual contributions of various multipole terms to the power radiated by multipoles. For calculating of multipole contributions and by formula (2), we integrated current densities excited in the dielectric ring obtained by simulation in CST Microwave Studio for frequencies close to resonance. Figure 4(a) clearly demonstrates that the choice of multipole decomposition is correct. The RCS values calculated by CST and those extracted from the multipole decomposition coincide. The fraction of the scattered radiation of magnetic and electric dipoles and quadrupoles obtained by computer modeling and the experimentally measured spectrum of the magnetic dipole are shown in Fig. 4.

As it seen from simulation results, in the vicinity of resonance, scattering mainly determined by intensity of magnetic dipole, then, experimentally measured resonant peak sufficiently confirmed high scattering of magnetic field from dipole. The contribution to the scattering of other multipoles is small and its share is 2×10^{-3} of the scattering of the magnetic dipole.

Simulated of electric and magnetic field distributions in the ring cross section are given in Figs. 5(a) and 5(b). Electric field is strongly concentrated inside of the dielectric ring [Fig. 5(a)] and significantly attenuated from 1 mm distance outside ring. One can assume the circular displacement currents flowing through dielectric ring and this distribution can be considered analogously to the distribution of conductivity currents in metallic rings. Magnetic field is concentrated in the free region in the center of rings [Fig. 5(b)].

Simulated results of the magnetic field vector distributions and their amplitudes in different cross sections above ring surface

Vol. 13 No. 2 | Imp. Factor: 8.13
DOI: https://doi.org/10.5281/zenodo.15845927

are shown in Figs. 6(a)–6(d). From Figs. 6(c) and 6(d), is following that the higher the plane is located above the ring, the more distant from ring axis, H-field vector is beginning to change direction to opposite, as it should be for magnetic dipole.

The resonant magnetic field amplitude have been measured at various distances between probe and ring plane (0; 5; 10; 15 ; 20 mm) and probe and ring axis (0 cm is the ring axis; 1.5; 2; 2.5 ; 3; 3.5; 4; 7; 12; 17; 22 cm). Figure 7 shows amplitude distributions along and perpendicular to the wave vector at a distance between ring and probe planes of 5 mm. The distance increased from ring plane for more than 20 cm leads to a sign change of magnetic field

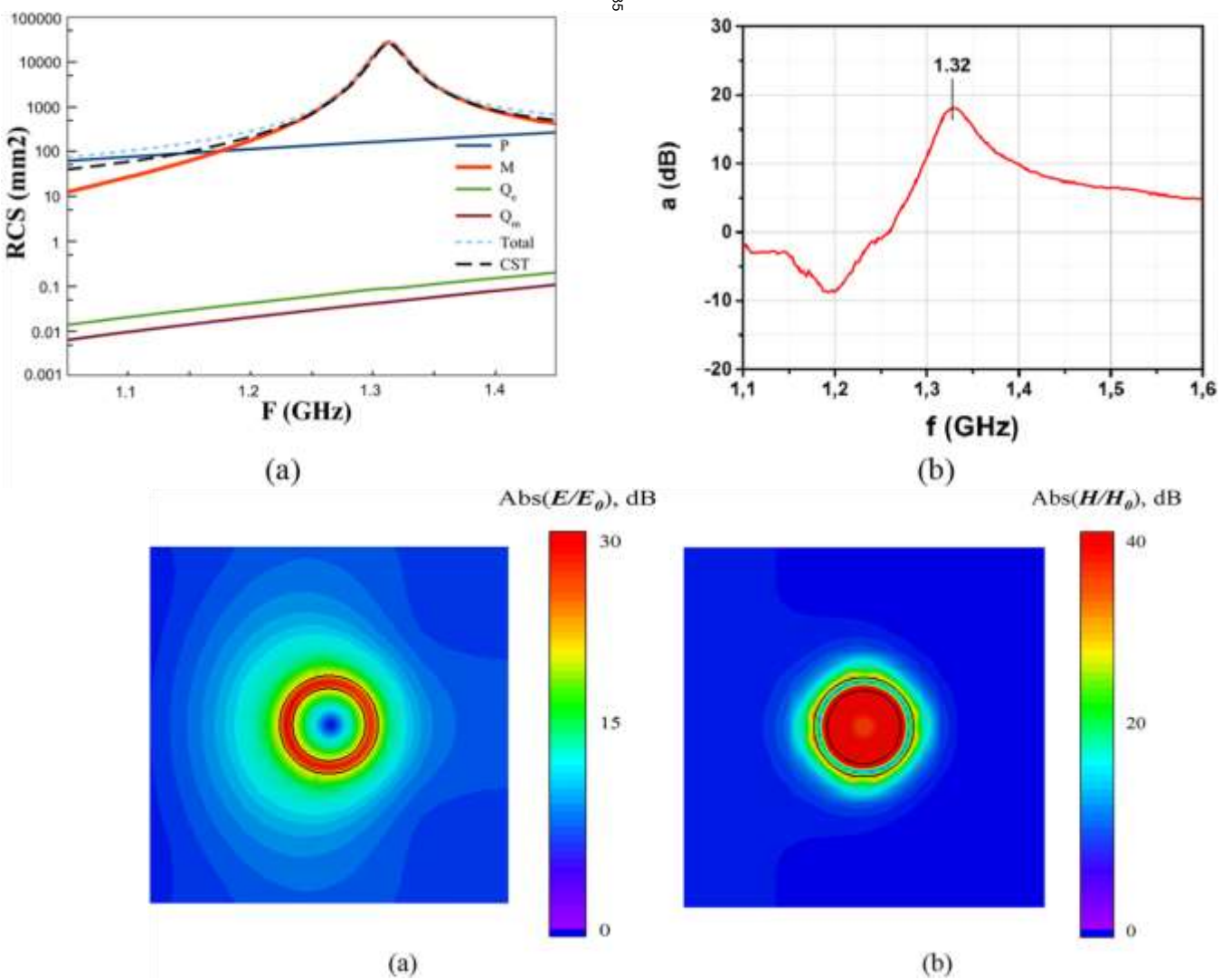

FIG. 4. Simulated (a) and experimental (b) scattering characteristics of the dielectric ring. P—electrical dipole; M—magnetic dipole; Q_e—electrical quadrupole; Q_m—magnetic quadrupole; Total—the scattering intensity by all multipoles.

FIG. 5. Central cross section of electric (a) and magnetic (b) field distribution in the ring.

Vol. 13 No. 2 | Imp. Factor: 8.13
DOI: https://doi.org/10.5281/zenodo.15845927

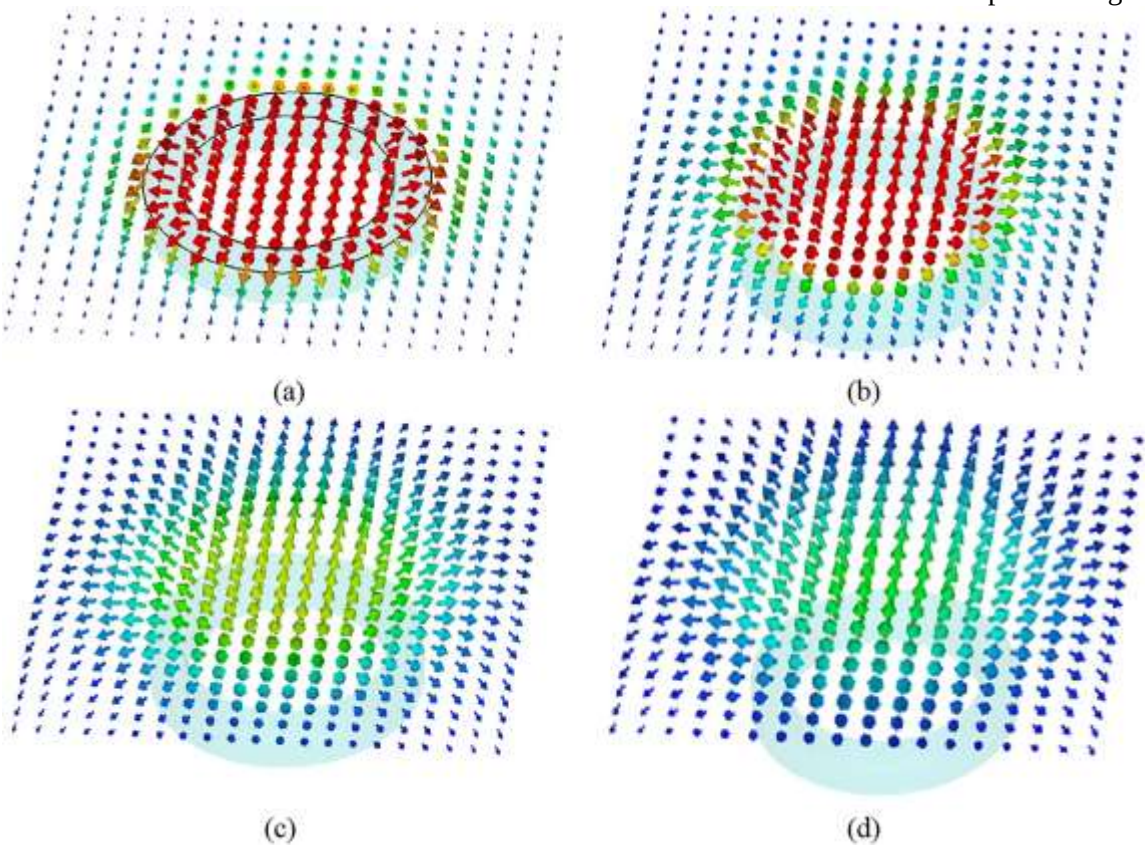

FIG. 6. Vector distribution of the magnetic field in the longitudinal section of the ring at the different distance h from its upper plane. (a) 0 mm; (b) 5 mm; (c) 10 mm; (d) 15 mm.

in accordance with phase shift of the magnetic component of incident wave and field scattered from magnetic dipole, which is completely consistent with the simulation results [Fig. 6(b)]. As it can be seen from simulated [Fig. 6(b)] and measured magnetic field [Fig. 7(b)], measured fields diminish with increased distance between ring and probe planes that corresponds to a decrease of the magnetic field of dipole.

Experimental (smoothed) and calculated curves for the distance between ring and probe planes of 5 mm are shown in Fig. 8.

The maximum amplitude of the resonant magnetic field is maximal in the center of the ring, which is consistent with the simulation results (Fig. 8). Moving the probe along the wave vector leads to an asymmetry of the distribution depending on the difference of the incident wave at the location of the probe (Fig. 7). For the same reason, a discrepancy is observed in Fig. 8 the difference between the measured and simulated fields, which does not exceed 4 dB (Fig. 8). We assume that the difference between the experimental and calculated CST curves may arise due to losses present in the ceramic material, errors in determining the permittivity and the loss tangent, large geometric dimensions of the ring under study, as well as the small diameter of the hole of the magnetic field probe and its thickness, which leads to distortion of the measured fields near the boundaries of the ring. Unfortunately, the manufacturer does not provide all the geometric parameters of the probe. Rough estimates made with a sensor ring thickness of 1 mm.

Vol. 13 No. 2 | Imp. Factor: 8.13
DOI: https://doi.org/10.5281/zenodo.15845927

To demonstrate the change in inclination angle of the dipole magnetic scattered field vector H, we carried out measurements with two mutually perpendicular orientations of the probe contour: in the first, the probe plane was perpendicular to the magnetic vector H_0 of the incident wave, in the second, the probe plane was parallel to the vector H_0 and perpendicular to the electric vector E_0 of the incident wave. The measurement results for the first orientation of the probe will be presented first, and then for the second. Figure 9 shows experimentally measured spectra when moving the probe along a straight line perpendicular to the wave vector k and parallel to the vector E_0 at a distance of 1 mm from the ring plane to the plane of the probe. The probe plane is perpendicular to the magnetic vector H_0 of the incident wave.

The amplitude of the magnetic field is maximal in the center of the ring, which is consistent with the field distribution for the magnetic dipole (Fig. 9, curve 19 mm). This increase in amplitude occurs due to the fact that the probe simultaneously registers the magnetic field H_0 of the incident wave and the magnetic field H scattered by the ring, which are collinear at this point. When the probe is moved, the inclination angle between the probe plane and the dipole magnetic vector H changes, and the total magnetic flux through the probe decreases. In the case when the probe is located at the ring edge (Fig. 9, 19 mm curve), the measured resonant signal is small, because the lines of the magnetic field vector H at this point are parallel to the plane of the ring and parallel to the plane of the probe, therefore the magnetic flux scattered by the ring

Radiation scattered at angles less than 14° will pass through the sensor only if there are one or more reflections from the inner wall of the probe, which will lead to a nonlinear attenuation of the signal from a cosine dependence to a sinusoidal one, which we observe (Fig. 8). The asymmetry of the experimental curve in Fig. 8(a) is explained by the non-parallelism of the ring plane and the probe plane, and in Fig. 8(b), the phase shift between incident and scattered wavesmost likelyplays a major role.

through the probe contour is small. When the probe is removed further from the ring, the resonant amplitude of the measured signal increases, despite the fact that the magnetic field amplitude has decreased, While the resonant peak has a minimum value, which is explained by a change in the direction of the vector H (Fig. 9, curve 30 mm).

Figure 10 shows the spectra measured by the probe at the dis tance of 3 mm from the outside of the ring. The probe moves along

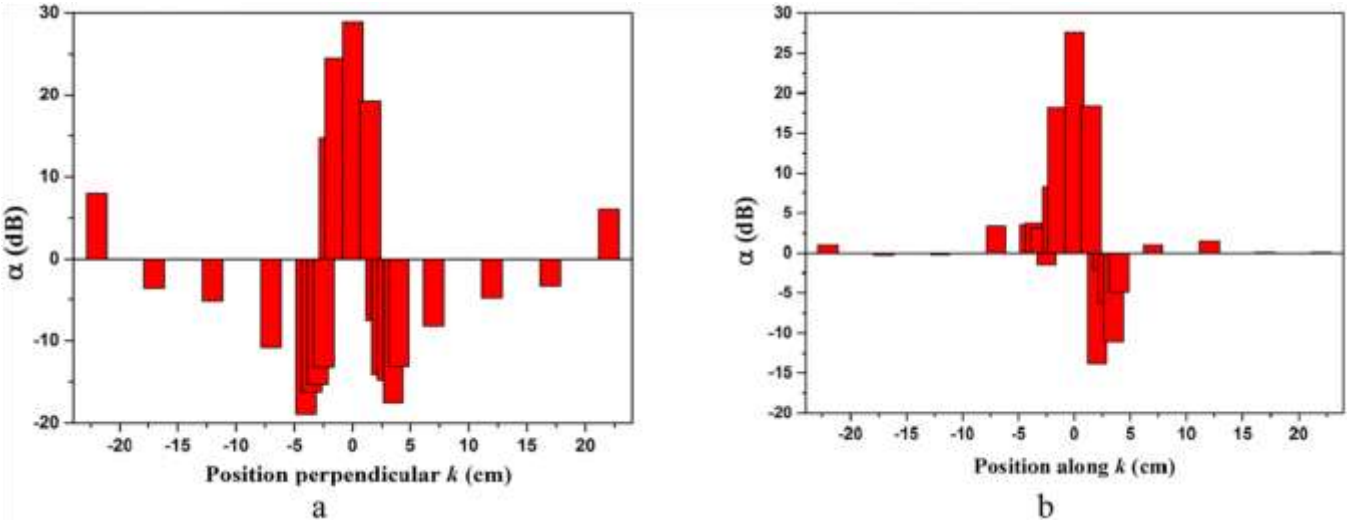

FIG. 7. Resonant amplitudes measured on different distances from ring center perpendicular to wavevector. The distance between ring and probe planes of 5 mm.

Vol. 13 No. 2 | Imp. Factor: 8.13
DOI: https://doi.org/10.5281/zenodo.15845927

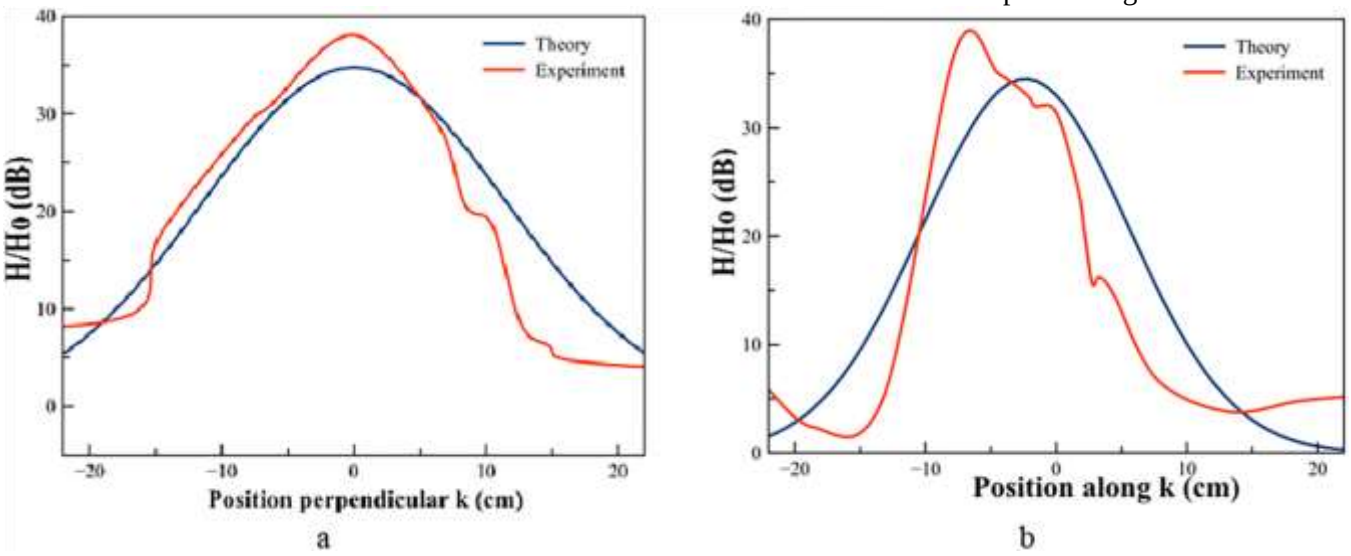

FIG. 8. Measured (smoothed) and simulated resonant amplitudes at different distances from ring center perpendicular (a) and along (b) to wave vector k. The distance between ring and probe planes of 5 mm.

the incident wave vector H_0 and the probe plane is perpendicular to H_0. In this case, as in the previous one, the probe signal is determined by the vector sum of H_0 and H. The signal value is maximum in the ring center (Fig. 10, curve 0 mm). When the probe is moved, the measured value decreases and with sufficient distance from the

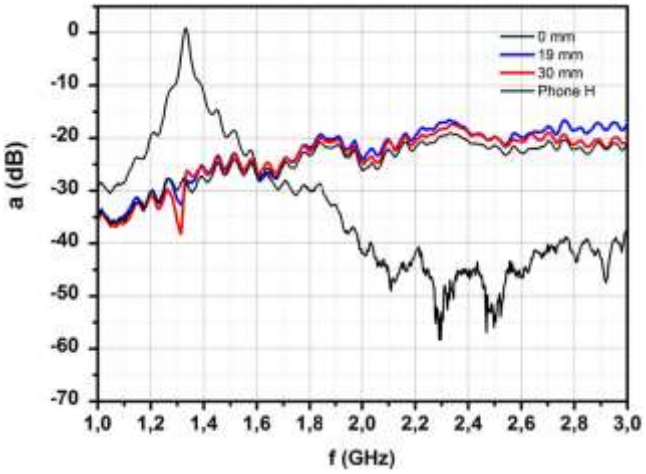

Vol. 13 No. 2 | Imp. Factor: 8.13
DOI: https://doi.org/10.5281/zenodo.15845927

because the flux of the magnetic field of the dipole changes sign and, accordingly, enters the plane of the probe from the reverse side. These changes are clearly visible in Fig. 6. Since the signal is strongly attenuated, it seems that the measured amplitude of the resonant field of the dipole is large, but in reality this is already the influence of noise.

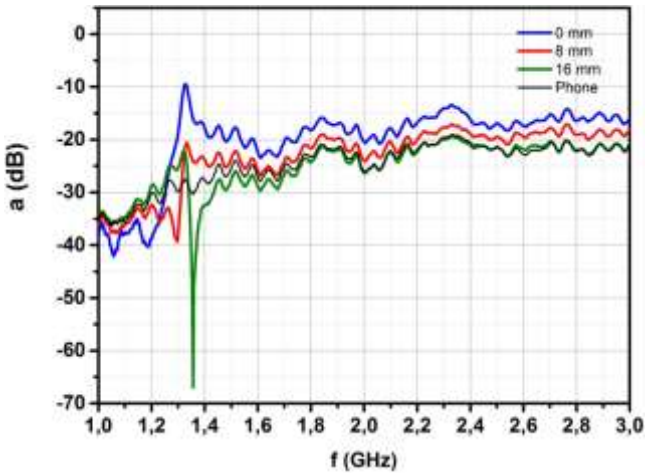

plane, the measured signal is minimal (Fig. 10, curve 16 mm),

FIG. 9. Measured spectra at different distances of the ring center taking 0 mm as the center of the ring, 19 mm as the outer edge of the ring, 30 mm—behind the ring, phone as spectra without ring. The probe plane is perpendicular to the magnetic component H_0 of the incident wave. The probe is assumed moving perpendicular to wavevector of incident wave and parallel to its E_0 component at a distance of 1 mm from the ring surface to the bottom edge of the sensor.

Here, phone is spectrum measured without a ring. Amplitude is indicated in dB.

FIG. 10. The measured spectra of probe displacement along magnetic component H_0 of the incident wave on the distance 3 mm from the ring edge to the probe center. The distance from the ring plane to the probe plane is 0; 8; and 16 mm.

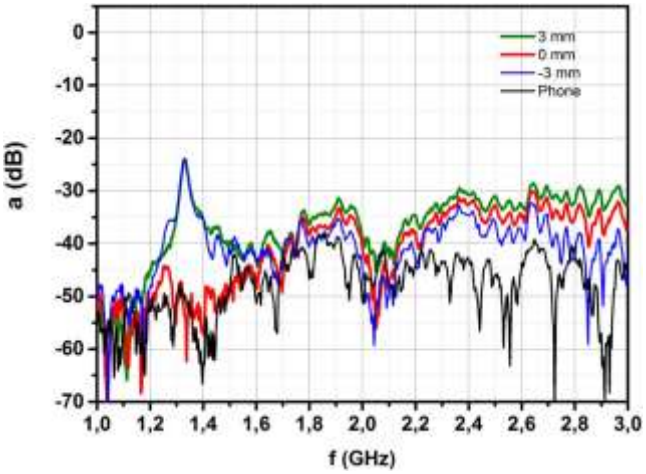

Vol. 13 No. 2 | Imp. Factor: 8.13
DOI: https://doi.org/10.5281/zenodo.15845927

FIG. 11. Measured spectra of the magnetic field for probe plane oriented perpendicular to electric field E_0. Probe is moved along the electric component E_0 line to 1 mm from the outer side of ring to the probe plane. Measuring points are 0 mm is for middle of the ring thickness; 3 mm—distance from the upper plane of the ring; −3 mm—distance from the ring plane; Phone—spectra without a ring.

The measurement spectra with the probe plane orientation along the magnetic vector H_0 and perpendicular to the electric field vector E_0 of the incident wave are shown in Fig. 11. In this case, the magnetic probe does not register the magnetic field signal of the incident wave H_0. The movement of the probe is similar to Fig. 10 along the vector H_0 at a distance of 1 mm from the outer surface of the ring to the plane of the probe. At the 0 mm point, the magnetic vector of the ring with current is parallel to the ring wall and parallel to the probe plane, so the signal is small (Fig. 11, 0 mm curve) and close to the background (Fig. 11, Phone curve). At distances of 3 mm from the lower and upper planes of the ring, the magnetic field vector of the ring is almost perpendicular to the probe plane, and the resonant amplitude is large. Therefore, we see two almost identical spectra with the large amplitude of the resonant peak, as it should be due to the symmetry of the magnetic fields at equal distances from the central plane of the ring.

IV. CONCLUSION

As a result of our research, we have shown:

- The dielectric ring has a significantly smaller set of multipole magnetic resonances, which leads to an increase in the share of excitation of dipole radiation compared to rectangular, elliptical, and spherical dielectric resonators.[40,41,51] The dielectric with the high permittivity with circular currents of displacement of the GHz band is an almost ideal magnetic dipole for the main resonance of scattering of incident radiation. The scattering fraction of all other multipoles is insignificant and is less than 2×10^{-3} of the main magnetic dipole resonance.
- Based on the obtained measurement and simulation results, we have demonstrated the applicability of the Bio–Savart–Laplace law not only for an annular circuit with a conduction current, but also for a dielectric annular circuit with the displacement current in the GHz range. The validity of the Bio–Savart–Laplace law for a dielectric ring circuit means that the displacement current flows in the body of the annular dielectric in a similar way to the conduction current in a metal ring.
- Calculations of the resonant frequency using expressions for capacitance and self-induction give the correct results, which can serve as a justification for using calculations of self-induction circuits of various geometric shapes.
- The dielectric ring can be used as the magnetic dipole to create various microwave structures, structures for “magnetic” manipulation of light in photonics.

ACKNOWLEDGMENTS

The theoretical study of this work was supported by the Basis Foundation for the Advancement of Theoretical Physics and Mathematics (Grant No. 23-1-1-61-2). The experimental study of this work was supported by the Ministry of Science and Higher Education of the Russian Federation (State Assignment No. 075-00269-25-00). The authors acknowledge support by the
Federal Academic Leadership Program, Priority 2030 (NUST MISIS Grant No. K2-2022-025).

[1] A. B. Evlyukhin, C. Reinhardt, A. Seidel, B. Luk’yanchuk, and B. N. Chichkov, “Optical response features of Si-nanoparticle arrays,” Phys. Rev. B 82(4), 045404 (2010). [3] A. García-Etxarri, R. Gómez-Medina, L. S. Froufe-Pérez, C. López, L. Chantada, F. Scheffold, J. Aizpurua, M. Nieto-Vesperinas, and J. J. Sáenz, “Strong magnetic response of submicron silicon particles in the infrared,” Opt. Express 19, 4815 (2011).

Vol. 13 No. 2 | Imp. Factor: 8.13
DOI: https://doi.org/10.5281/zenodo.15845927

AUTHOR DECLARATIONS

Conflict of Interest

The authors have no conflicts to disclose.

Author Contributions

Mikhail M. Bukharin: Software (equal); Visualization (equal). Leonid M. Vasilyak: Conceptualization (equal); Formal analysis
(equal); Funding acquisition (equal); Methodology (equal); Project administration (equal); Writing – review & editing (equal). Alexey Basharin: Methodology (equal); Writing – original draft (equal); Writing – review & editing (equal). Boris Luk`yanchuk: Formal analysis (equal); Funding acquisition (equal); Writing – review & editing (equal). Anar Ospanova: Software (equal); Visualization (equal). Vladimir Ya. Pecherkin: Data curation (equal);
Investigation (equal); Validation (equal); Writing – review & editing (equal).

DATA AVAILABILITY

The data that support the findings of this study are included within the article.

REFERENCES

Bakker, R. M., Yu, Y. F., Paniagua-Domínguez, R., Luk'yanchuk, B., & Kuznetsov, A. I. (2017). Resonant light guiding along a chain of silicon nanoparticles. Nano Letters, 17(6), 3458–3464. https://doi.org/10.1021/acs.nanolett.7b00416

Baryshnikova, K. V., Smirnova, D. A., Luk'yanchuk, B. S., & Kivshar, Y. S. (2019). Optical anapoles: Concepts and applications. Advanced Optical Materials, 7(12), 1801350. https://doi.org/10.1002/adom.201801350

Basharin, A., Chuguevsky, V., Volsky, N., Kafesaki, M., & Economou, E. N. (2017). Extremely high Q-factor metamaterials due to anapole excitation. Physical Review B, 95(3), 035104. https://doi.org/10.1103/PhysRevB.95.035104

Cappello, B., Ospanova, A. K., Matekovits, L., & Basharin, A. A. (2020). Mantle cloaking due to ideal magnetic dipole scattering. Scientific Reports, 10, 2413. https://doi.org/10.1038/s41598-020-59126-w

Cao, L., White, J. S., Park, J. S., Schuller, J. A., Clemens, B. M., & Brongersma, M. L. (2009). Engineering light absorption in semiconductor nanowire devices. Nature Materials, 8, 643–647. https://doi.org/10.1038/nmat2477

Coenen, T., van de Groep, J., & Polman, A. (2013). Resonant modes of single silicon nanocavities excited by electron irradiation. ACS Nano, 7(2), 1689–1698. https://doi.org/10.1021/nn304550g

Vol. 13 No. 2 | Imp. Factor: 8.13
DOI: https://doi.org/10.5281/zenodo.15845927

Evlyukhin, B., Novikov, S. M., Zywietz, U., Eriksen, R. L., Reinhardt, C., Bozhevolnyi, S. I., & Chichkov, B. N. (2012). Demonstration of magnetic dipole resonances of dielectric nanospheres in the visible region. Nano Letters, 12(7), 3749–3755. https://doi.org/10.1021/nl301594s

Fu, Y. H., Kuznetsov, A. I., Miroshnichenko, A. E., Yu, Y. F., & Luk'yanchuk, B. (2013). Directional visible light scattering by silicon nanoparticles. Nature Communications, 4, 1527. https://doi.org/10.1038/ncomms2538

Kapitanova, P., Ternovski, V., Miroshnichenko, A., Pavlov, N., Belov, P., Kivshar, Y., & Tribelsky, M. (2017). Giant field enhancement in high-index dielectric subwavelength particles. Scientific Reports, 7, 731. https://doi.org/10.1038/s41598-017-00837-0

King, N. S., Li, Y., Ayala-Orozco, C., Brannan, T., Nordlander, P., & Halas, N. J. (2011). Angle- and spectral-dependent light scattering from plasmonic nanocups. ACS Nano, 5(9), 7254–7262. https://doi.org/10.1021/nn202109v

Klimov, V. (2014). Nanoplasmonics (1st ed.). Jenny Stanford Publishing.

Kuznetsov, I., Miroshnichenko, A. E., Fu, Y. H., Zhang, J. B., & Luk'yanchuk, B. (2012). Magnetic light. Scientific Reports, 2, 492. https://doi.org/10.1038/srep00492

Luk'yanchuk, B., Paniagua-Domínguez, R., Kuznetsov, A. I., Miroshnichenko, E., & Kivshar, Y. S. (2017). Suppression of scattering for small dielectric particles: Anapole mode and invisibility. Philosophical Transactions of the Royal Society A, 375(2090), 20160069. https://doi.org/10.1098/rsta.2016.0069

Miroshnichenko, E., Evlyukhin, A. B., Yu, Y. F., Bakker, R. M., Chipouline, A., Kuznetsov, A. I., Luk'yanchuk, B., Chichkov, B. N., & Kivshar, Y. S. (2015). Nonradiating anapole modes in dielectric nanoparticles. Nature Communications, 6, 8069. https://doi.org/10.1038/ncomms9069

Nemkov, N. A., Stenishchev, I. V., & Basharin, A. A. (2017). Nontrivial nonradiating all-dielectric anapole. Scientific Reports, 7, 1064. https://doi.org/10.1038/s41598-017-01145-9

Ospanova, A. K., Labate, G., Matekovits, L., & Basharin, A. A. (2018). Multipolar passive cloaking by nonradiating anapole excitation. Scientific Reports, 8, 12514. https://doi.org/10.1038/s41598-018-30708-3

Vol. 13 No. 2 | Imp. Factor: 8.13
DOI: https://doi.org/10.5281/zenodo.15845927
Papasimakis, N., Fedotov, V. A., Savinov, V., Raybould, T. A., & Zheludev, N. I. (2016). Electromagnetic toroidal excitations in matter and free space. Nature Materials, 15(3), 263–271. https://doi.org/10.1038/nmat4569

Person, S., Jain, M., Lapin, Z., Sáenz, J. J., Wicks, G., & Novotny, L. (2013). Demonstration of zero optical backscattering from single nanoparticles. Nano Letters, 13(4), 1806–1809. https://doi.org/10.1021/nl4005018

Traviss, D. J., Schmidt, M. K., Aizpurua, J., & Muskens, O. L. (2015). Antenna resonances in low aspect ratio semiconductor nanowires. Optics Express, 23(17), 22771–22782. https://doi.org/10.1364/OE.23.022771

Tribelsky, M. I., & Miroshnichenko, A. E. (2016). Giant in-particle field concentration and Fano resonances at light scattering by high-refractive-index particles. Physical Review A, 93(5), 053837. https://doi.org/10.1103/PhysRevA.93.053837

van de Groep, J., Coenen, T., Mann, S. A., & Polman, A. (2016). Direct imaging of hybridized eigenmodes in coupled silicon nanoparticles. Optica, 3(1), 93–96. https://doi.org/10.1364/OPTICA.3.000093